Chapter 2
Investigation of a Renewable Energy-Based Integrated System for Baseload Power Generation

Mehdi Hosseini, Ibrahim Dincer and Marc A. Rosen

Abstract A renewable energy-based integrated system is proposed for baseload power generation. Wind, solar, and biomass options are considered. The electric power produced by wind turbines, a photovoltaic (PV) system, and fuel cells is fed to the power grid. The surplus electricity produced by the integrated energy system is stored in forms of compressed air and hydrogen. When required, the compressed air is heated in a combustion process and expanded in a gas turbine for further power generation. The hydrogen produced by the electrolysis process is fed to a solid oxide fuel cell (SOFC) system for electricity generation. The system is analyzed with energy and exergy methods, and results are presented for monthly power generation, compressed air energy storage (CAES) and compression, and hydrogen production and consumption rates. Moreover, exergoeconomic analyses are performed based on the unit exergy cost of the electricity produced by the integrated system. The round-trip efficiency of the CAES system is 60 % without considering heat recovery potentials. The overall energy and exergy efficiencies of the integrated system are 37.0 and 31.9 %, respectively. Results of the exergoeconomic analyses show that the unit cost of electricity generated by the Wind-CAES system is 7 ¢/kWh, while it is 89 and 17 ¢/kWh for the photovoltaic-hydrogen-solid oxide fuel cell and the biomass-solid oxide fuel cell-gas turbine systems, respectively.

Keywords Renewable · Integrated energy system · Energy · Exergy · Solar · Wind · Biomass · Fuel cell

M. Hosseini (✉) · M. A. Rosen
Faculty of Engineering and Applied Science, University of Ontario Institute
of Technology, 2000 Simcoe St. North, ON L1H 7K4, Canada
e-mail: mehdi.hosseini@uoit.ca

I. Dincer
Department of Mechanical Engineering, University of Ontario Institute
of Technology (UOIT), 2000 Simcoe Street North, Oshawa ON L1H 7K4, Canada
e-mail: ibrahim.dincer@uoit.ca

2.1 Introduction

Renewable energy resources (e.g. wind and solar) cannot produce steady electric power, due to their intermittent characteristics. Wind speed and direction change almost constantly due to weather conditions, and solar irradiance reaching the surface of the earth is dependent on geographical location, time of the day, and clearness of the sky. However, proper design of wind turbines (variable speed power generators, appropriate pitching and tilting) makes them capable of producing a fixed-rated power over a course of wind speed range. No matter how sophisticated are the wind turbine control systems, the power output of a wind park depends on the wind speed. Therefore, when utilizing wind turbines in a baseload power plant, the intermittent power output of the wind park must be compensated. One solution is using energy storage systems, and example of which is compressed-air energy storage (CAES). During the period of excess power generation by the wind park, a CAES system can convert and store the surplus electricity in the form of compressed air.

Another option for overcoming the intermittent behavior of wind energy in generating constant rated power is hydrogen storage. According to Yang and Aydin [1], the excess power output of wind turbines can be utilized in water electrolysers for hydrogen production and storage. Once the hydrogen is stored in an appropriate high-pressure vessel, it can be used in a combustion engine, fuel cell, or water-cooled burner to produce high-quality steam for space heating, or to drive a turbine to generate electric power. In large scale baseload power generation, the size of the hydrogen tanks will be significantly large, and work of compression will be considerable.

Batteries, as small scale power generation systems, could be a good option to store the excess generated electricity by the wind turbine(s) and meet the demand when needed. However, in large scale scenarios (baseload power), batteries are very bulky, expensive, and require continuous maintenance. CAES seems promising, since the compressed air is stored in abandoned mines or underground salt caverns. CAES utilizes the familiar gas turbine cycle, with a simple modification. When integrated with wind turbines, excess generated electricity by the wind turbines is consumed by the compressors to compress ambient air, which is stored in the salt cavern or the abandoned mine.

Solar energy systems can also benefit from energy storage. The surplus electric power output of a solar photovoltaic (PV) system can be utilized for hydrogen production, which can be stored in hydrogen tanks for later use. Integrated wind and solar energy-based systems can help reduce greenhouse gas emission rates, if designed for baseload power production. This is achieved through diminishing the use of fossil fuels for electricity generation. Further, Ashraf, et al. [2] report that solar photovoltaic systems have great potential in grid-connected power generation, due to their simplicity of installation, operation and maintenance, and being carbon emission free electricity generation systems.

However, not all the renewable energy resources are emission free. Unlike wind and solar that produce almost no greenhouse gases (GHGs), biomass is a renewable energy resource that releases carbon containing gases when used. For example, a solid-oxide fuel cell-micro gas turbine (SOFC-GT) system integrated with biomass

gasification releases 741 g/kWh of CO_2 [3]. This level of gross emission is comparable to the carbon dioxide emission by a fossil fuel power plant, 617 g/kWh.

Renewable energy-based systems can be integrated to increase renewable energy utilization. Depending on the available renewable resources, different configurations can be proposed. In this study, an integrated renewable energy-based system is proposed to supply baseload electric power. The system utilizes wind, solar, and biomass as the renewable energy resources. Basedload wind energy is the subject of the work by Greenblatt, et al. [4]. The economic feasibility of a wind-CAES system is investigated and compared with gas and wind-gas power plants. The CAES system is used to store the surplus generated electricity by the wind turbines. For one set of input assumptions, i.e. $ 5/GJ effective natural gas price and 650 W/m² wind resource, the wind-CAES is the most expensive (6 ¢/kWh) system. This result is obtained for a compressed air energy storage system with a 169 h storage capacity.

Residential applications of photovoltaic electricity generation systems can be grid-connected and grid-independent. In both cases energy storage systems may be required to increase renewable energy utilization and/or to achieve higher power reliability. Widén, et al. [5] present options for improving PV capability in load following scenarios, considering the following options: PV array orientation, demand-side management (DSM) and electricity storage. They apply the available methods to a PV system for residential applications, and conclude that energy storage is more efficient than DSM and photovoltaic orientation methods if high PV penetration is desired. Castillo-Cagigal, et al. [6] present active demand-side management (ADSM) analysis for a grid-connected residential PV system in Spain. The ADSM method basically controls the power load variations between the electricity generation/supplying systems and the demand. The presented experimental set up is connected to the local electricity grid, and takes advantage of lead-acid battery storage.

Solar PV systems also can be used for large-scale, baseload power generation, as pointed out by Radchik, et al. [7].They state that intermittency of solar power output is a major factor in economic development of baseload PV systems. They propose market-based solutions for baseload PV electricity generation systems integrated with virtual non-intermittent generators, i.e. gas-fired power plants. This provides a financially attractive option for integrating a solar generator into existing electricity markets.

Solid oxide fuel cells are capable of operating with such fuels as natural gas, hydrogen, and syngas. The latter is produced with biomass gasification, and can be directly used after post-processing in SOFCs [3]. Colpan, et al. [8] investigate effects of gasification medium on systems integrating biomass gasification and SOFCs. Steam gasification is found to have a higher exergy efficiency, relative to air gasification. Also, the results show that a higher electricity generation rate (in the SOFC) is achieved with steam as the biomass gasification medium. Exergy, a measure of the quality of energy, is a concept that helps with identifying sources of irreversibility in a system or a process flow [9]. Exergy combines with economics to form exergoeconomics, which is used for evaluating the costs related to unit exergy flows and system products [9].

In the present study an integrated renewable energy-based system is investigated for baseload power generation. The integrated system utilizes wind, solar and
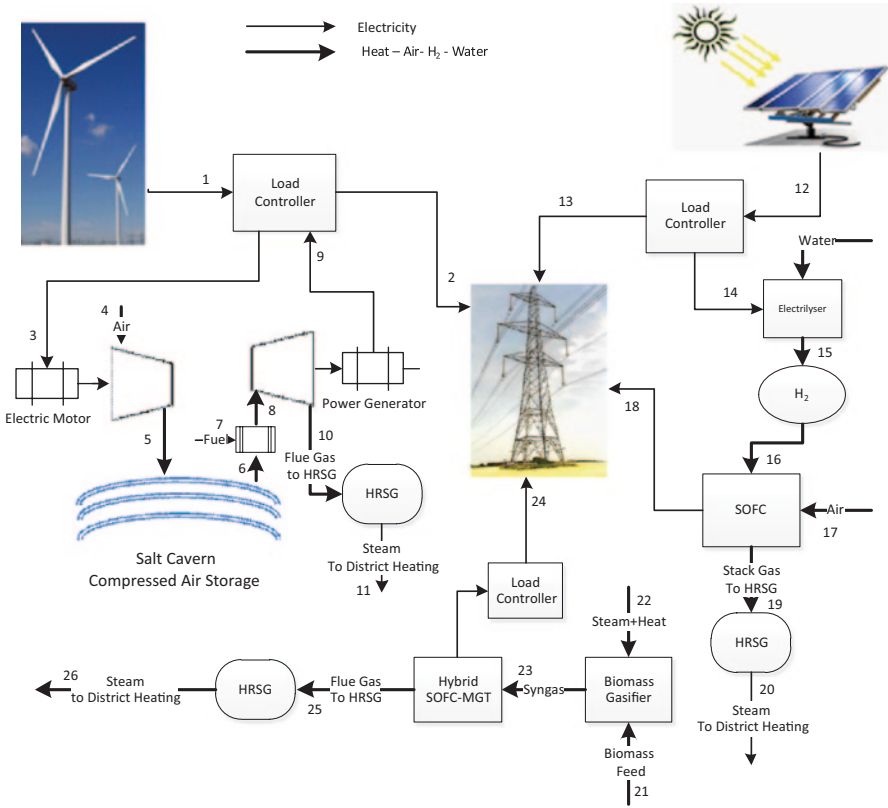
Fig. 2.1 Simplified schematic of grid-integrated renewable combined heat and power system for a district

biomass as the renewable energy resources. Energy and exergy methods are used to analyze the system electric power generation and thermal energy output. Moreover, carbon emission rates are calculated on a per kWh basis. Economic analyses are combined with exergy concepts to perform exergoeconomic analyses of the system, providing information regarding unit cost of electricity production of the electric power generation components.

2.2 System Description

The renewable-based integrated energy system contains three different power generation systems, each utilizing a renewable energy resource. As shown in Fig. 2.1, wind, solar and biomass are the renewable energy resources.

The integrated system is meant to supply the baseload electric power of a district, and the system components are selected so the wind park has the greatest share in

meeting the power demand. The operation of each sub-system of the integrated system is described below.

Wind-CAES

The power output of the wind park (point 1) is fed to a load controller. The controller decides if the power output should be delivered to the grid (point 2) or to the CAES system (point 3). When the electric power output of the wind park is more than the demand, the surplus electricity is fed to the CAES system. The compressor consumes the surplus electricity to pressurize ambient air (point 4) in two steps. First, the ambient air is compressed to a medium pressure (pressure ratio of r_c), and is cooled in the heat-exchanger. The heat removed from the compressed air in the heat exchanger can be used for district heating, or can be stored in a thermal storage system. The medium pressure, low temperature air enters the next compressor for further compression. During the compression process it gains energy. To decrease the required volume for storage, the high pressure compressed air is cooled in the second heat exchanger, and stored in underground salt caverns (point 5).

If the power output of the wind park is less than the demand, the gas turbine operates, extracting compressed air (point 6) from the salt cavern. The compressed air enters a combustion process with natural gas (point 7), and is fed to the gas turbine (point 8) for electric power generation (point 9). To increase efficiency, the gas turbine exhaust gas (point 10) is fed to the heat recovery steam generator (HRSG) for low pressure steam generation (point 11). The generated steam is stored in a thermal energy storage system. Due to the intermittency of power generation by the gas turbine, an advantageous way to utilize the generated steam is energy storage, as it gives more flexibility in meeting part of the thermal demand of the district. The compressor must produce enough compressed air so there is a net positive amount of stored air in the salt cavern throughout the year, considering air consumption by the gas turbine.

PV-H$_2$-FC System

The photovoltaic-hydrogen-solid oxide fuel cell (PV-H$_2$-FC) is considered to supply a small part of the electricity demand (5 MW). This decision is made due to the high land use of the photovoltaic system (5.9 m^2/kWe). The electricity output of the PV system depends on solar irradiance, which is related to climate. It is possible to size the PV system so that electricity generated during day time exceeds demand, and surplus electricity can be harvested and stored as hydrogen gas. Thus the PV system generates as much electricity as needed to meet the electricity demand. The intermittent characteristic of solar energy is overcome by the hydrogen–fuel cell system. The electrolyser utilizes the surplus electricity of the PV system (point 13) during times of the day when PV output exceeds the electricity demand of the grid. The

electrolyser splits water (point 14) into hydrogen and oxygen (point 15). Interest in the substitution of fossil fuels with hydrogen is growing; however hydrogen storage is a challenge in developing sustainable energy systems. Hydrogen can be stored and transported in bulk as a compressed gas or liquid, and new storage methods are under development. These storage methods require significant inputs through compression and liquefaction processes, and require high-tech storage tanks. In contrast, on-site utilization of hydrogen eliminates most of these difficulties. In the system illustrated in Fig. 2.1, hydrogen is produced in an electrolyser installed at the PV-H$_2$-FC site. Therefore, there is no need for long term storage of hydrogen, because it is consumed by the fuel cell system on demand. Moreover, with proper sizing of system components, high pressure compressed gas is not required. The stored hydrogen is fed (point 16) to the SOFC system for electricity generation (point 18).

Solid oxide fuel cells are capable of generating baseload electric power. In addition, the high temperature exhaust gases leaving the fuel cell stack (point 19) can be used for space heating or hot water production in a heat utilization unit. Since the fuel cell is in operation only when required, the heat gained by the heat utilization unit is stored in a thermal energy storage system (point 20).

Biomass-SOFC-GT System

The integrated system includes a biomass gasification unit, an SOFC, a gas turbine and a heat recovery unit. Wood dust or crop waste is used as biomass in the biomass gasification unit (point 21). To improve the performance of the gasification process, the moisture content of the biomass feed is controlled via a biomass dryer. Various drying methods are available, among which direct steam biomass drying has the higher exergy efficiency. The superheated steam is supplied by the heat recovery steam generator. The gasification process occurs in the presence of pressurized steam (point 22). The product syngas (point 23) is fed to the fuel cell system for power generation (point 24). The gases leaving the fuel cell stack enter the combustion chamber of the micro gas turbine, and the gas turbine cascade for further electricity generation. The biomass-SOFC-GT system is assumed to supply a fixed portion of the electricity demand of the grid. This means that, in contrast to the wind-CAES and PV-H$_2$-FC systems, the biomass-SOFC-GT system has steady, not-intermittent, operation. The SOFC-GT exhaust gas feeds a heat recovery steam generator (point 25) for further renewable energy utilization. The generated steam is fed to the thermal storage system for thermal management (point 26).

Thermal Energy Storage

The heat recovered from the gas turbine flue gas of the CAES and SOFC-GT systems is stored in the form of hot water in thermal energy storage systems. The hot water is used for hot water usage or space heating.

2.3 Energy and Exergy Analyses

The main components of the integrated system are considered in the energy and exergy analyses. Their energy and exergy flows are illustrated in the following section.

Wind Park

Wind energy is a cubic function of wind speed. Therefore, any fluctuation in the wind speed leads to a significant change in its available energy. Wind turbines are usually in operation 80% of the year, and produce nearly 30% of their nominal power capacity throughout the year [10]. Wind power density (W/m^2) is an index quantifying the level of wind resource, and can be related to the cube of wind speed and the Weibull distribution function. The efficiency of wind turbines is limited to a maximum of 59%, known as the Betz limit [10].

Power output of the wind turbine is a function of wind speed, blade geometry and turbine efficiency, and can be expressed as

$$\dot{W}_{wt} = \frac{\pi}{8} C_p \rho D^2 v^3 \tag{2.1}$$

Here, C_p is the wind turbine efficiency, which is related to aerodynamics characteristics of the blades [11]. Due to the quality of electric power output of the wind turbine, the energy and exergy efficiencies are the same; therefore, the exergy destruction rate of the wind turbine is calculated using:

$$\dot{I}_{wt} = \left(\frac{1}{C_p} - 1\right)\dot{W}_{wt} \tag{2.2}$$

Compressed Air Energy Storage System

Compressor

The energy and exergy balances for the CAES compressor and intercoolers, respectively, follow:

$$(\dot{m}_{air} h_{air})_{in} + (\dot{m}_{air} w_C)_{in} = (\dot{m}_{air} h_{air})_{out} \tag{2.3}$$

$$(\dot{m}_{air} ex_{air})_{in} + (\dot{m}_{air} w_C)_{in} = (\dot{m}_{air} ex_{air})_{out} + \dot{I}_c \tag{2.4}$$

The enthalpy of air is calculated as $\Delta h = c_p \Delta T$, where ΔT is obtained using the isentropic relations for the compressor:

$$T_{\text{out}} = T_{\text{in}} \left[1 + \frac{1}{\eta_{\text{c}}} \left(r_{\text{c}}^{\frac{\gamma_{\text{air}} - 1}{\gamma_{\text{air}}}} - 1 \right) \right] \tag{2.5}$$

For a compression ratio r_c and a known inlet air temperature, the compressor outlet temperature is calculated. The specific work of compression can thus be calculated as follows:

$$w_{\text{c}} = (h_{\text{air}})_{\text{in}} - (h_{\text{air}})_{\text{out}} \tag{2.6}$$

In Eq. 2.4, exergy of the inlet air to the compressor is zero, considering the ambient conditions be the same as the reference environment. The balances for the air intercoolers are as follows:

$$(\dot{m}_{\text{air}} h_{\text{air}})_{\text{in}} + (\dot{m}_{\text{cw}} h_{\text{cw}})_{\text{in}} = (\dot{m}_{\text{air}} h_{\text{air}})_{\text{out}} + (\dot{m}_{\text{cw}} h_{\text{cw}})_{\text{out}} \tag{2.7}$$

$$(\dot{m}_{\text{air}} ex_{\text{air}})_{\text{in}} + (\dot{m}_{\text{cw}} ex_{\text{cw}})_{\text{in}} = (\dot{m}_{\text{air}} ex_{\text{air}})_{\text{out}} + (\dot{m}_{\text{cw}} ex_{\text{cw}})_{\text{out}} + \dot{I}_{\text{intercooler}} \tag{2.8}$$

where subscript cw in Eqs. 2.7 and 2.8 represents the cooling water, removing heat from the compressed air.

Gas Turbine

The energy and exergy balances for the gas turbine of the CAES system, respectively, follow:

$$(\dot{m}_{\text{air}} h_{\text{air}})_{\text{in}} + (\dot{m}_{\text{fuel}} LHV_{\text{CH}_4})_{\text{in}} = (\dot{m}_{\text{gas}} w_{\text{T}})_{\text{out}} + (\dot{m}_{\text{gas}} h_{\text{gas}})_{\text{out}} \tag{2.9}$$

$$(\dot{m}_{\text{air}} ex_{\text{air}})_{\text{in}} + (\dot{m}_{\text{fuel}} ex_{\text{CH}_4})_{\text{in}} = (\dot{m}_{\text{gas}} w_{\text{GT}})_{\text{out}} + (\dot{m}_{\text{gas}} ex_{\text{gas}})_{\text{out}} + \dot{I}_{\text{GT}} \tag{2.10}$$

The enthalpy of the combustion gases is calculated as $h = c_{p,g} T$, where T is obtained using the isentropic relations for the gas turbine:

$$T_{\text{out}} = T_{\text{in}} \left[1 + \frac{1}{\eta_{\text{GT}}} \left(r_{\text{T}}^{\frac{\gamma_{\text{g}} - 1}{\gamma_{\text{g}}}} - 1 \right) \right] \tag{2.11}$$

The air and gas specific heats are functions of gas molar fractions, and temperature.

Energy and Exergy Efficiencies of the Wind-CAES System

The main output of the integrated renewable energy-based system is baseload electric power. The system takes advantage of heat recovery to increase renewable energy utilization. Since the energy resources are renewable, and therefore intermittent, the recovered heat is stored as hot water in thermal energy storage systems. The inputs to the Wind-CAES section of the integrated system are wind and natural gas. The overall energy and exergy efficiencies follow:

$$\eta_{\text{wind-CAES}} = \frac{W_{\text{demand}} + Q_{\text{HRSG}} + (\Delta m \cdot h)_{\text{stored air}}}{E_{\text{Wind}} + (m \cdot LHV)_{\text{CH}_4}} \qquad (2.12)$$

$$\psi_{\text{wind-CEAS}} = \frac{W_{\text{demand}} + Ex_{\text{q,HRSG}} + (\Delta m \cdot ex_{\text{ph}})_{\text{stored air}}}{Ex_{\text{Wind}} + (m \cdot ex)_{\text{CH}_4}} \qquad (2.13)$$

Here, $P_{\text{demand}}, Ex_{\text{q,HRSG}}, and \Delta m_{\text{stored air}}$ account for the total annual electric energy demand of the wind park, the total annual heat recovery from the overall CAES system, and the difference between production and consumption of compressed air on a yearly basis, respectively. The energy inputs in the denominator of the efficiency equations are also considered on a yearly basis. The notations in Eq. 2.13 explain the exergy terms using the same concepts.

PV-H₂-FC system

The mathematical model and energy and exergy analysis equations for the PV-H₂-FC system are presented by the authors elsewhere [12].

The PV cell power output is a function of its terminal voltage and current, which are dependent on solar irradiance and ambient temperature:

$$\dot{W}_{\text{PV}} = IV \qquad (2.14)$$

The difference between PV electric power output and the grid electric power demand is

$$\Delta \dot{W}_{\text{PV}} = \dot{W}_{\text{PV}} - \dot{W}_{\text{demand}} \qquad (2.15)$$

If $\Delta \dot{W}_{\text{PV}} > 0$, the PV system produces more power than the demand, and the surplus electricity is fed to the electrolyser for hydrogen production. If $\Delta \dot{W}_{\text{PV}} < 0$, the SOFC produces power to make up for the power difference between the PV and the grid.

Energy and Exergy Efficiencies of the PV-H$_2$-FC System

The energy input to the hybrid PV-fuel cell system is solar irradiance. Although solar energy is not available during night hours and cloudy days, the system operates solely on solar energy, thanks to the storage options considered in the integrated system. The main output of the system is electricity, which is fed to the grid. Heat recovery from the SOFC stack gas is another output of the system. The integrated system is sized to supply the electricity demand throughout the year. Therefore, the storage tank size should always contain enough hydrogen to feed the fuel cell, when required. On a year round basis, hydrogen production is set to be more than hydrogen consumption. Thus, the remaining hydrogen in the storage tank is another output of the system. The overall energy and exergy efficiencies of the hybrid PV-fuel cell system can be written as follows:

$$\eta_{PV-fuel\ cell} = \frac{W_{demand} + Q_{HRSG} + \Delta m_{H_2}\ LHV}{E_{solar}} \tag{2.16}$$

$$\psi_{PV-fuel\ cell} = \frac{W_{demand} + Ex_{q,HRSG} + \Delta m_{H_2}\ ex_{ch,H_2}}{Ex_{solar}} \tag{2.17}$$

In Eq. 2.16, W_{demand} is the annual electricity demand in kWh, Q_{HRSG} is the total heat recovery from the fuel cell stack gas, Δm_{H_2} is the difference between production and consumption of hydrogen on a yearly basis, and E_{solar} is the annual solar energy received by the PV system. The notations in Eq. 2.17 apply to the exergy terms similarly.

Biomass Gasification and SOFC-GT

Details of the modeling and thermodynamic analysis of the hybrid SOFC-GT system integrated with biomass gasification are presented by the authors elsewhere [13]. The electric power output of the biomass-SOFC-GT system is expressible as

$$\dot{W}_{SOFC-MGT} = \dot{W}_{SOFC}\eta_{conv} + \dot{W}_{MGT} - \dot{W}_{airC} - \dot{W}_{consumption} \tag{2.18}$$

where η_{conv} is DC/AC power converter, and $\dot{W}_{airC}$ and $\dot{W}_{consumption}$ are air compressor and internal consumption, respectively.

The energy and exergy balances can be written as follows:

$$(\dot{m}ex)_{biomass} + \dot{Ex}_{steam} + \dot{Ex}_Q = \dot{W}_{SOFC-MGT} + \dot{Ex}_{out} + \dot{I}_{biomas-SOFC-MGT} \tag{2.19}$$

Here, $\dot{Ex}_{steam}$ is the exergy rate of steam entering the gasifier, $\dot{Ex}_Q$ is the gasification thermal exergy rate, and $\dot{Ex}_{out}$ is the exergy rate of the flue gas of the SOFC-GT cycle, which is released to the environment.

Accounting for the heat recovered in the HRSG, the total efficiencies of the SOFC-GT CHP system are

$$\eta_{\text{biomass-SOFC-GT}} = \frac{W_{\text{demand}} + Q_{\text{HRSG}}}{(m \cdot LHV)_{\text{biomass}} + E_{\text{Steam}} + Q_{\text{gasifier}} + E_{\text{gas-cleaning}}} \quad (2.20)$$

$$\psi_{\text{biomass-SOFC-GT}} = \frac{W_{\text{demand}} + \text{Ex}_{\text{Q,HRSG}}}{(m.ex)_{\text{biomass}} + Ex_{\text{Steam}} + Ex_Q + Ex_{\text{gas-cleaning}}} \quad (2.21)$$

Overall Energy and Exergy Efficiencies of the Integrated Renewable Energy-Based System

The overall energy and exergy efficiencies of the integrated renewable energy-based system for baseload power generation follow:

$$\eta_{\text{wind-PV-biomass}} = \frac{W_{\text{demand}} + Q_{\text{HRSG}} + \Delta m_{\text{H}_2} LHV_{\text{H}_2}}{E_{\text{solar}} + E_{\text{Wind}} + (m \cdot LHV)_{\text{biomass}}} \quad (2.22)$$

$$\psi_{\text{wind-PV-biomass}} = \frac{W_{\text{demand}} + Ex_{\text{q,HRSG}} + \Delta m_{\text{H}_2} ex_{\text{ch,H}_2}}{Ex_{\text{solar}} + Ex_{\text{Wind}} + (m \cdot ex)_{\text{biomass}}} \quad (2.23)$$

Here, W_{demand}, $Ex_{\text{q,HRSG}}$, and Δm_{H_2} account for the total annual electric energy demand, thermal exergy recovery from all the available waste heat sources, and the difference between production and consumption of hydrogen on a yearly basis, respectively.

Exergoeconomic Analysis

In economic calculations of energy systems, unit costs based on energy are conventionally used. Since these systems are incur losses that can be better quantified based on exergy concepts, the use of exergy based unit costs better distribute costs among outputs. The combination of exergy analysis and economic calculations represents a useful tool for optimization of energy systems, and forms the basis of the relatively new field of exergoeconomics. The exergy model calculates the exergy content of each point in the system, and the economic model accounts for all costs

relevant to capital, operation and maintenance (O&M) of the system. In the exergo-economic models, each exergy stream has a cost. Thus, the cost of exergy of all inlet streams plus the capital and O&M costs equals to the cost of exergy of all exiting streams [9].

The exergoeconomic factor f relates the costs associated with exergy destruction and exergy losses to the levelized capital costs. The exergoeconomic factor of component k, f_k, is defined as

$$f_k = \frac{\dot{Z}_k}{\dot{Z}_k + c_{F,k}(\dot{I}_k + \dot{Ex}_{loss})} \tag{2.24}$$

where $c_{F,k}$ is the unit cost of exergy of fuel provided to the component. The values of the exergoeconomic factor fall between zero and one. A small value for f suggests that the system needs to be improved in terms of irreversibility, although this may require capital cost investments. Higher values for f signify that, no matter how efficient the component is, its purchase cost is significantly high. The concepts of exergoeconomic analysis discussed in this section are applied to the components of the integrated systems.

2.4 Assumptions and Data

The modeling and analyses are performed based on the following assumptions and data.

- Transient behavior of the systems is not considered, although the weather data has transient characteristics.
- The wind turbine power output is 3.5 MW, with a $ 700/kW capital cost [4].
- The CAES system is considered to have 168 h of air storage capacity.
- The equivalent natural gas price (natural gas plus carbon dioxide emission price) is $ 5/GJ.
- The compression pressure range for the parametric study is 81, 64, and 49 bar.
- The expansion pressure range for the parametric study is 64, 49 and 36 bar.
- Hourly wind speed data of Port Colbourne, Ontario, Canada [14] are used for wind power calculations.
- Hourly solar irradiance data of Toronto [15], Ontario, Canada are used for PV power calculations.
- The reference environment state, taken as similar to the ambient condition, for the exergy analysis is set to 1 bar and 298 K.

Economic and exergoeconomic analyses are performed based on data presented in Table 2.1.

Table 2.1 Unit cost of components

Component	Wind turbine	Air compressor	Gas turbine	PV	SOFC	Electrolyser	Bio-SOFC-GT
Capital cost, $/kW	700[a]	175[a]	185[a]	5400[b]	2300[c]	590[d]	3800[e]

[a] Data adapted from Greenblatt et al. (2007)
[b] Data adapted from SunPower Corporation (2012), N. Enbar (2010)
[c] Data adapted from Braun et al. (2011), McIlveen-Wright et al. (2011)
[d] Data adapted from state-of-the-art hydrogen production (2009)
[e] Data adapted from McIlveen-Wright et al. (2011)

2.5 Results and Discussion

The investigation of the integrated renewable energy-based baseload power generation system is performed for 5 MW solar PV and 25 MW biomass-SOFC-GT power outputs. Since each sub-power generation system is independent from the rest, the results are presented separately. In this section the results of modeling, and energy and exergy economic analyses of the systems are presented. When discussing the monthly performance of the Wind-CAES system, the compression ratio of the compressor stages is set to 8, while the expansion ratio of each stage of the gas turbine is considered to be 6. The pressure difference between the compressed air storage system and the gas turbine operating pressure is regulated by a pressure regulator, considering the pressure losses in the pathways and pipelines [4].

Wind-CAES system

The Wind-CAES system power output accounts for 94% of the baseload power supply. However, since wind power is inherently intermittent, the shares of the wind park and the CAES systems in providing the grid with electricity vary. Power penetration is the ratio of the electricity provided by the system to the electric power demand. Power penetrations for the wind park and the CAES system are shown in Fig. 2.2. There is no specific trend to the shares of the two power supply systems, since they strongly depend on the wind resource. However, the wind park plays a major role in the Fall-Winter months.

Figure 2.2 also shows that power penetration of the wind park for some months of the year is more than 100%. During these months, the power output of the wind park exceeds the demand; however, the CAES system is fully charged, so there is no need to compress air with the electricity. In some analyses, the wind park excess electricity is dissipated or used for space heating, unless there is the possibility of selling the electricity to the grid.

The CAES system is charged (refilled with compressed air) when the wind park power output exceeds the electricity demand. It is discharged when there is a need for power production otherwise met by the gas turbine. Therefore, the charging/
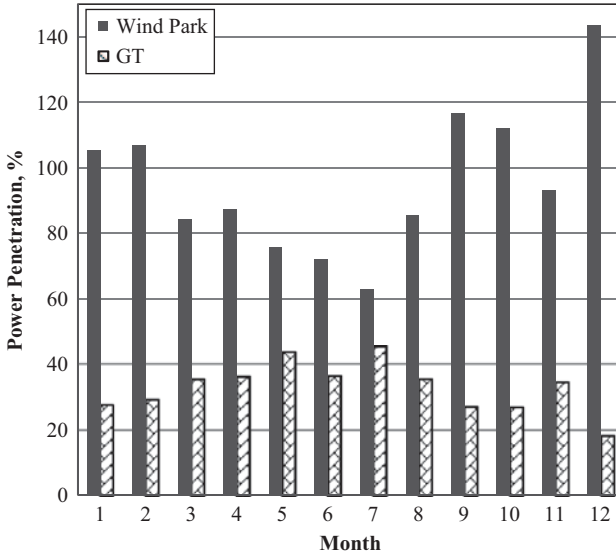
Fig. 2.2 Monthly power penetration of wind park and gas turbine sites ($r_c=8$, $r_{GT}=6$, $h_s=168$)

discharging rates change as illustrated in Fig. 2.3. The system component (wind turbines, air compressor, gas turbine) capacities are selected to maintain a net positive quantity of stored air in the cavern throughout the year. The data in Fig. 2.3 is presented in million kg of compressed air per month, to quantify the differences between storage and consumption for each month.

Wind-CAES systems are generally not carbon emission-free power generation plants. In fact, if the compressed air is heated by combustion, some levels of carbon and other greenhouse gas emissions are released. In this paper, the compressed air undergoes a combustion process with methane. Figure 2.4 illustrates monthly changes in fuel consumption and carbon dioxide emissions. They are proportional to the gas turbine operation and the need for excess power generation.

With the performance of the Wind-CAES system described, a parametric study is performed considering changes in the compressor and gas turbine pressure ratios. For a fixed storage cavern pressure at 64 bar (implying a compressor stage pressure ratio of 8, since two compression stages are considered), the change in the wind power penetration is shown in Fig. 2.5, for various gas turbine pressure ratios. Figure 2.5 shows that the wind park penetration decreases as the gas turbine pressure ratio increases.

A higher pressure ratio in the gas turbine results in a higher specific power output. Therefore, fewer wind turbines are required for the wind park, and the share of the gas turbine in meeting the electricity demand increases (Fig. 2.6).

The gas turbine expansion ratio impacts the capacity of the main components of the Wind-CAES system, which affects related system costs. The unit cost of electricity is a function of the system total capital and maintenance costs and the total generated power by the system during its lifetime. Figure 2.7 shows that
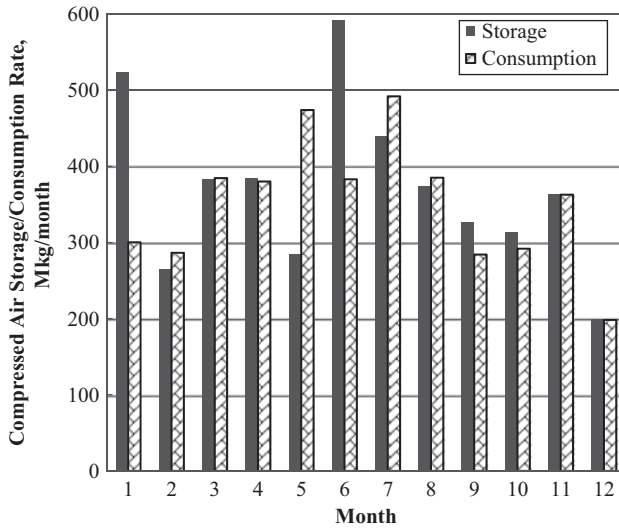
Fig. 2.3 Charging and discharging phases of the compressed air storage system ($r_c=8$, $r_{GT}=6$, $h_s=168$)
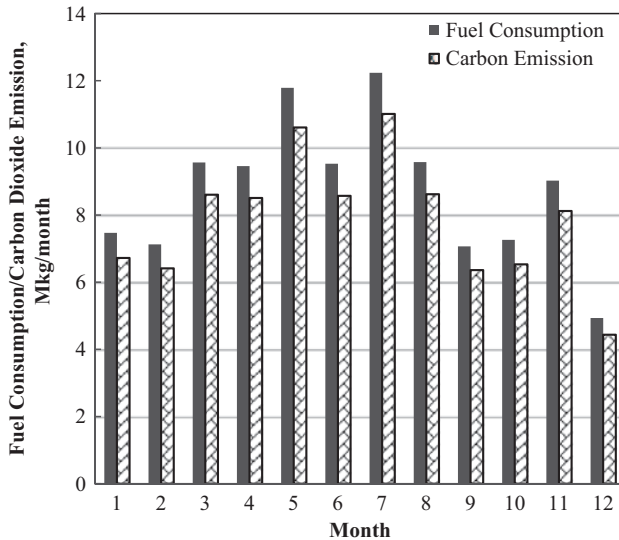

Fig. 2.4 Fuel consumption and carbon dioxide emission rates ($r_c=8$, $r_{GT}=6$, $h_s=168$)

increasing the GT expansion ratio decreases the unit cost of generated electricity by the Wind-CAES system. According to Fig. 2.7, the unit cost of electricity drops from 7.4 to 7.0 ¢/kWh as the GT expansion ratio increases from 6 to 8. For a fixed GT capacity, a higher specific power output leads to lower air and fuel consumption. A decrease in the fuel consumption due to the increase in turbine
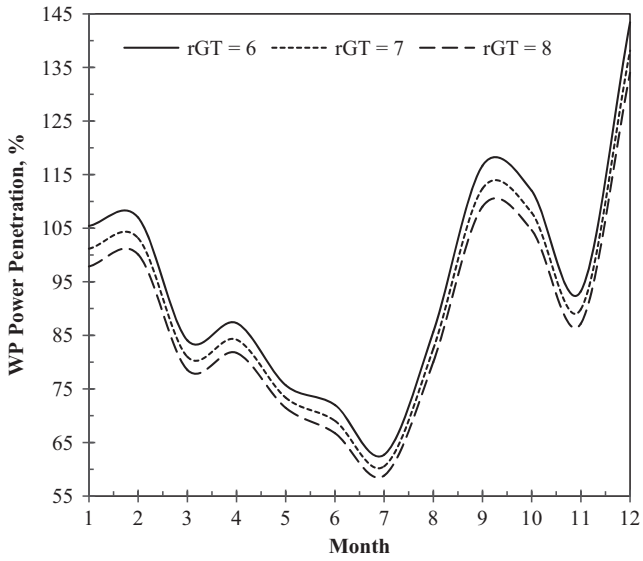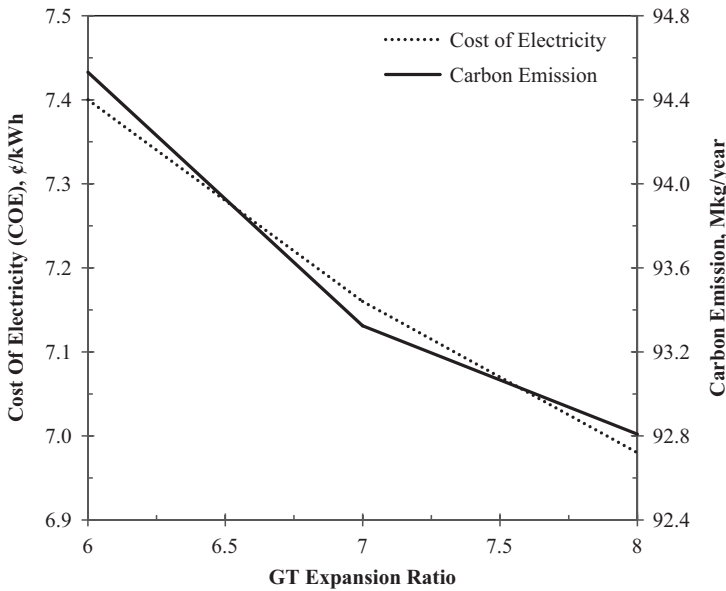
Fig. 2.5 Monthly power penetration of wind park with various GT expansion ratios ($r_c = 8$, $h_s = 168$)
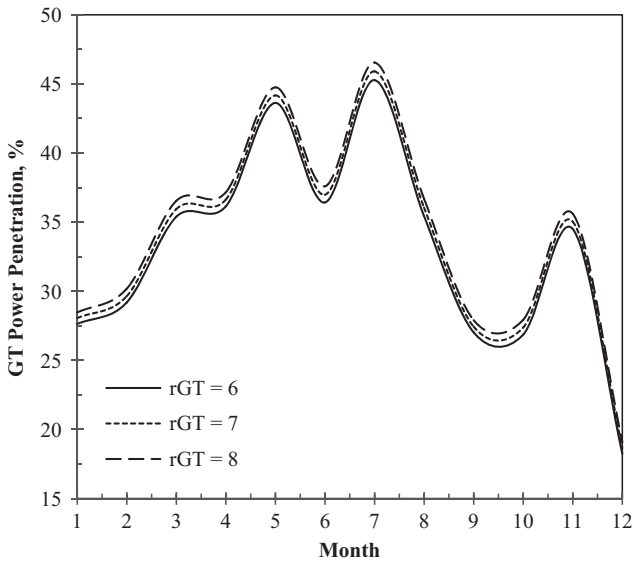
Fig. 2.6 Monthly power penetration of GT for various GT expansion ratios ($r_c = 8$, $h_s = 168$)

**Fig. 2.7** Cost of electricity (COE) and annual carbon emission vs. GT expansion ratio ($r_c=8$, $h_s=168$)

Table 2.2 Effect of gas turbine expansion ratio of the overall energy and exergy efficiencies of the Wind-CAES system ($r_c=8$, $h_s=168$)

Gas turbine expansion ratio	6	7	8
Wind-CAES energy efficiency, %	37.17	37.90	37.60
Wind-CEAS exergy efficiency, %	32.83	33.86	34.73

expansion ratio results in a reduction in the yearly carbon dioxide emissions, as also illustrated in Fig. 2.7.

Moreover, decreasing the pressure difference between the gas turbine inlet pressure and the pressure of the air storage cavern (i.e., increasing the gas turbine expansion ratio), increases the overall energy and exergy efficiencies of the Wind-CAES system, as observed in Table 2.2.

As discussed in Fig. 2.6 and illustrated in Fig. 2.8, the GT power output increases if the pressure of the air entering the turbine cascade is closer to the compressed air pressure (decreasing the level of pressure loss in the air cavern). Also, Fig. 2.7 shows that the annual carbon emission rate decreases with increasing gas turbine pressure ratio. However, since the share of the wind park in providing the grid with electricity decreases, the specific carbon dioxide emission in g/kWh increases. A trade-off between decreasing electricity generation cost and carbon emission can be the objective for an optimization problem.
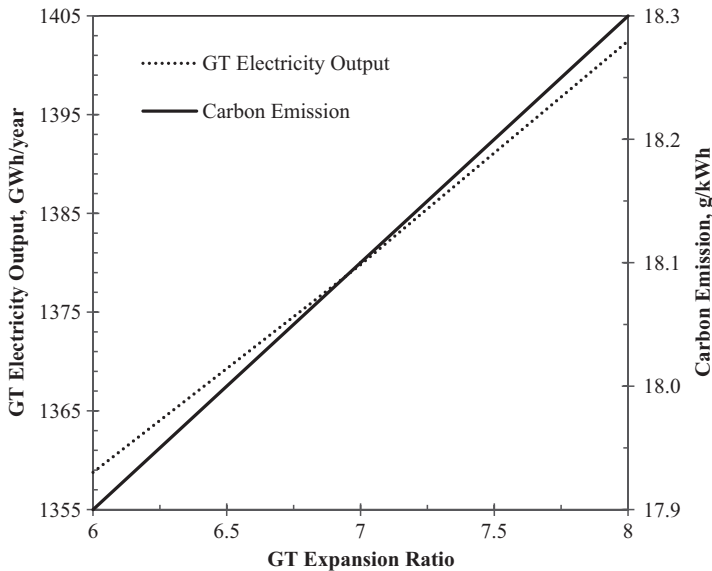
Fig. 2.8 GT electric power output and carbon emission per unit of Wind-CAES electric power vs. GT expansion ratio ($r_C = 8$, $h_s = 168$)

The exergoeconomic method is used to calculate the unit cost of exergy of the system components. Here, the unit cost of generated electricity by the gas turbine is presented. The compressed air pressure affects the electricity cost of the Wind-CAES system, mainly due to the changes in the system components' capacities. The variation of the unit cost of GT electricity output with a change in the pressure of the stored air and the expansion ratio of the gas turbine is shown in Fig. 2.9. The highest price is for the case when the difference between the compressed air pressure and the turbine inlet pressure is a maximum. Figure 2.9 shows that if there is no pressure difference between the storage system and the gas turbine inlet pressure, the unit cost of GT electricity output is a minimum.

PV-H$_2$-FC System

Hydrogen is produced by water electrolysis, using surplus generated electricity by the PV system, and is consumed by the solid oxide fuel cell when the PV power is below the demand.

The production/consumption pattern depends on the temporal variation of the solar irradiance. Figure 2.10 shows that more hydrogen is produced during high irradiance months (spring-summer) than Fall-Winter months. But, the SOFC consumes more hydrogen during low solar irradiance months. The system components are sized to have positive cumulative hydrogen in the storage tank throughout the year. The hydrogen production/consumption pattern is observed to be proportional
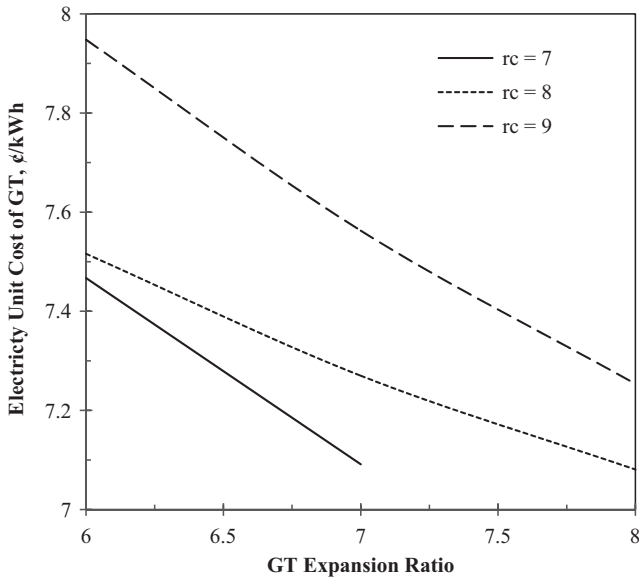
Fig. 2.9 Variation of GT unit cost of electric exergy with the compressed air pressure ratio and the gas turbine expansion ratio
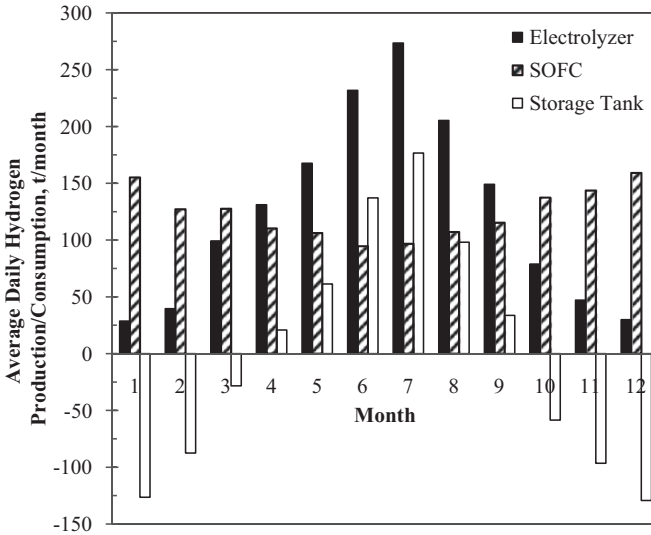

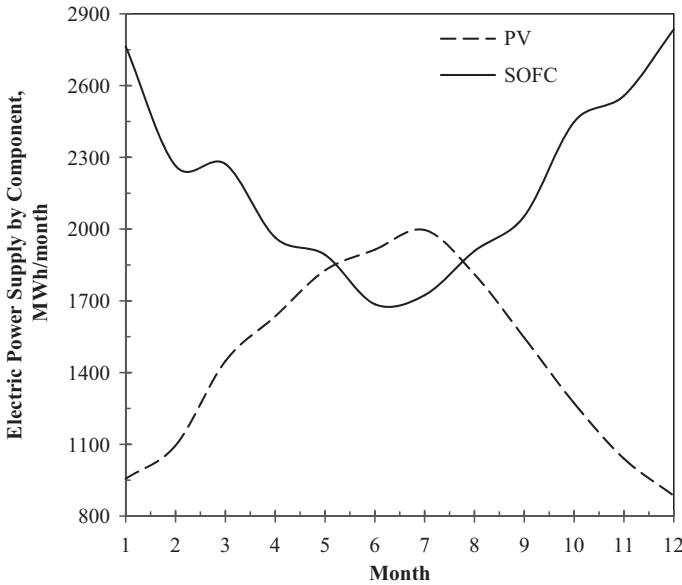**Fig. 2.10** Monthly flow rate of hydrogen production/consumption

Fig. 2.11 PV and SOFC share in electric power supply

to the PV and fuel cell power outputs (see Fig. 2.11). A better understanding of the PV and fuel cell shares in power production can be observed in Fig. 2.12. The power penetration of the PV system exceeds that of the fuel cell in Spring-Summer months, and exhibits an opposite trend in Fall-Winter months.

A graphical illustration of the contributions of the PV-H_2-FC system main components to the total exergy destruction (Fig. 2.13) shows that the PV accounts for almost 85 % of the annual exergy destruction. This is mainly associated with internal irreversibility.

Since the performance of the PV-H_2-FC system depends on the weather condition, for the exergoeconomic analysis, the unit cost of exergy of the products of the main components are determined on a monthly basis. Figure 2.14 shows that during the months with high solar irradiance, the cost of generated electricity by the PV and fuel cell systems is minimal. The PV electricity generation is significantly below its rated power during Fall-Winter months, causing a significant increase in the unit costs of the products.

Although the fuel cell operates closer to its nominal capacity during this period of time, the generated electricity is still expensive due to the higher price for hydrogen production in months with low solar irradiance.

Integrated Renewable Energy-based Power Generation System

PV has a very low exergoeconomic factor, demonstrating its high level of exergy destruction, according to Table 2.3. The SOFC in the PV-H_2-FC system has the min-
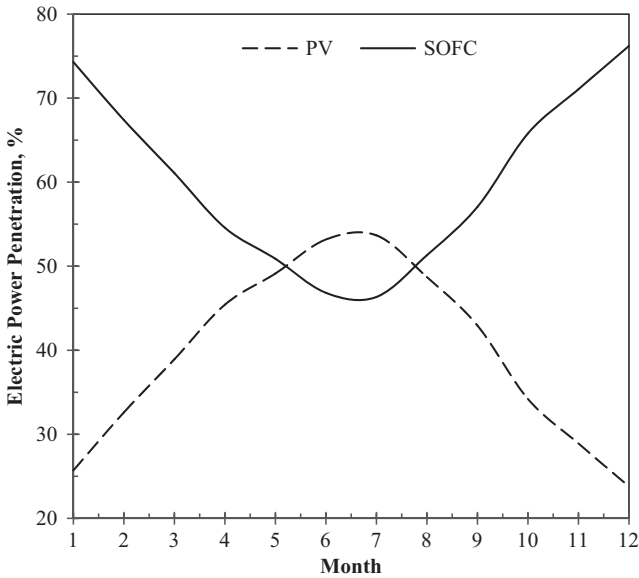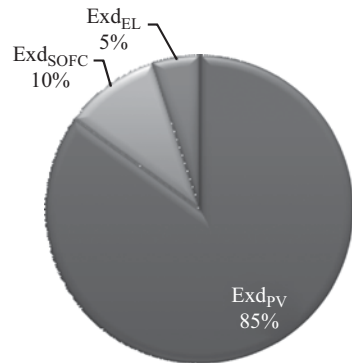
Fig. 2.12 Electric power penetration of PV and SOFC system in meeting the demand

Fig. 2.13 Annual exergy destruction breakdown for the main components of the PV-H$_2$-FC system

imum exergoeconomic factor due to its high exergy destruction and low capacity factor. The exergoeconomic factors of the other main components of the integrated renewable energy-based system are also presented in Table 2.3.

Table 2.4 provides information regarding heat recovery potential from the components of the integrated system. Moreover, the ratios of the heat recovered to the electric power input (output) of the components are presented. Table 2.4 shows that there is a good potential for heat recovery from the compressed air during compression and storage of air in the CAES system. The extent of heat recovery from the SOFC-GT system integrated with biomass gasification is significant, since heat can be recovered from the gasification process, the fuel cell and the micro gas turbine.
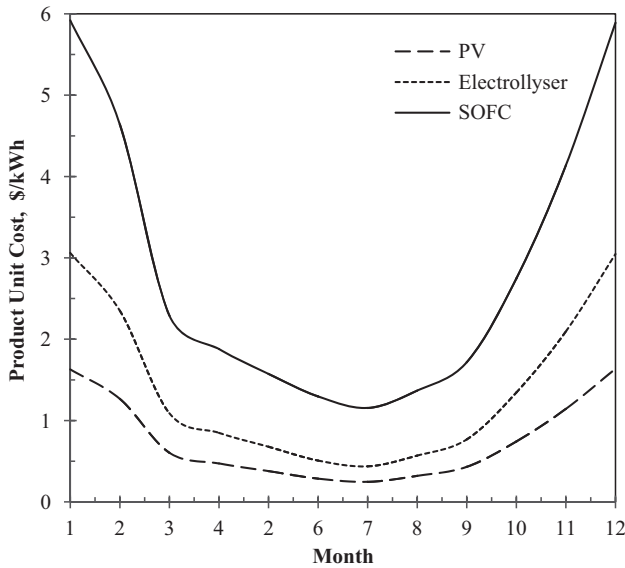
Fig. 2.14 Unit cost of exergy for PV-H$_2$-FC components' products

Table 2.3 Exergoeconomic factor for the main components of the integrated CHP system

Component	PV-H$_2$-FC			Wind-CAES			Biomass-SOFC-GT
	PV system	Electrolyser	SOFC	Wind park	Air compressor	Gas turbine	
Exergoeconomic factor	0.33	0.36	0.12	0.62	0.55	0.89	0.17

Table 2.4 Heat recovery from the integrated system components

Component	CAES[a]		PV-H$_2$-FC	Biomass-SOFC-GT
	Air	GT		
Heat recovery, GWh/y (GWh*th*/GWh*e*)	246.8 (0.3)	118.0 (0.1)	11.6 (0.3)	148.7 (0.7)
Energy consumption, GWh/y	817.3	1458.8	12.0[b]	687.0 (biomass)
Electric power output, GWh/y		1358.8	43.8	219.0

[a] $r_c = 8$, $h_s = 168$, $r_{GT} = 6$
[b] Energy for pre-heating the hydrogen feed to the SOFC

The round-trip efficiency of the CAES system can be calculated as $\dfrac{1358.8}{1458.8 + 817.3} = 60\%$ without considering heat recovery potentials. If the electrical equivalent of the heat recovered from the compression and expansion processes is considered (assuming 50% efficiency of a thermal power plant to calculate the equivalent electric energy for heat), the round-trip energy efficiency is 68%.

Table 2.5 Energy and exergy flows and efficiencies of the integrated system components

	Wind-CEAS	PV-H$_2$-FC	Biomass-SOFC-GT	Integrated system
E_{inlet}, GWh/y	13,600.0	614.0	609.7	14,823.7
E_{outlet}, GWh/y	5060.0	55.5	367.9	5483.4
η, %	37.2	9.0	60.3	37.0
Ex_{inlet}, GWh/y	13,900.0	568.6	646.45	15,115.3
Ex_{outlet}, GWh/y	4490.0	51.9	274.2	4816.1
ψ,%	32.3	9.1	42.4	31.9

Table 2.6 Unit cost of generated electricity by each sub-system of the integrated system

Sub-system	Wind-CAES	PV-H$_2$-FC	Integrated biomass-SOFC-GT
Unit cost of electricity, ¢/kWh	7.4[a]	89[b]	17[c]

[a] $r_c=8$, $h_s=168$, $r_{GT}=6$, $P_{GT}=470$ MW
[b] $P=5$ MW
[c] $P=25$ MW, $TIT=1300$ K, $T_{stack}=1173$ K

The total energy and exergy flows in the integrated renewable energy-based system are listed in Table 2.5. These values are reported for each sub-system and for the overall system, separately. Values of energy and exergy efficiencies are reported. Table 2.5 shows that the overall energy and exergy efficiencies of the integrated system are 37.0 and 31.9%, respectively. A lower exergy value of recovered heat is the main reason for the lower overall exergy efficiency, compared to the energy efficiency.

Each sub-system of the integrated renewable energy-based system generates electricity, however with a different unit cost of electricity. Table 2.6 reports the electricity generation cost by the integrated system. Results of the exergoeconomic analyses show that the unit cost of electricity generated by the Wind-CAES system is 7 ¢/kWh, while it is 89 and 17 ¢/kWh for the PV-H$_2$-SOFC and the biomass-SOFC-GT systems, respectively.

Conclusions

Integrated renewable energy-based systems have the potential for baseload power generation. The novel integrated system presented in this study utilizes wind, solar and biomass energy resources, and provides 500 MW baseload power. The performance of the integrated system depends on weather conditions and the system component design parameters. For a 64 bar compressed air pressure, and a 36 bar gas turbine inlet air pressure, 356 3.5-MW rated power wind turbines are required to generate 470 MW baseload power. The compressed air storage will have a volume 3.3×10^3 m^3 in and an energy storage capacity of 79 GWh (i.e., 7 days storage capacity at the gas turbine rated power).

The lower the pressure difference between the compressed air in the cavern and the gas turbine inlet air pressure, the fewer are the wind turbines required in the Wind-CAES system. This results in higher penetration for the gas turbine.

The results also show that 5.35×10^5 PV modules (covering 0.66 Mm^2 of land) are required to generate 5 MW of baseload electric power. The capacity of the SOFC of the PV-H$_2$-FC system is 5 MW with 11.6 GWh*th* annual heat-recovery potential. The PV system accounts for almost 85 % of the annual exergy destruction, due to its internal irreversibility.

Nomenclature

c_p	specific heat at constant pressure, kJ/kg.K
Cp	wind turbine effectiveness
D	diameter, m
ex	specific exergy, kJ/kg
Ex	exergy flow, kJ
$\dot{Ex}$	exergy flow rate, kW
f	exergoeconomic factor
h	specific enthalpy, kJ/kg
I	electric current, A
$\dot{j}$	exergy destruction rate, kW
LHV	lower heating value, kJ/kg
$\dot{m}$	mass flow rate, kg/s
Q	thermal energy, kJ
$\dot{Q}$	heat flow rate, kW
r	compression ratio, bar/bar
SC	steam to carbon ratio
T	temperature, K
v	velocity, m/s
V	voltage, V
w	specific work, kJ/kg
W	electric energy, kWh (kJ)
$\dot{W}$	electric power, kW
$\dot{Z}$	levelized capital cost rate, $/s

Greek Letters

ρ	density, kg/m^3
η	energy efficiency, %
ψ	exergy efficiency, %
γ	specific heat ratio

Subscripts

airC	air compressor
c	compressor
ch	chemical exergy
conv	electricity converter
cw	cooling water

CH_4	methane
DH	district heating heat demand
F	fuel
g	gas
GT	gas turbine
in	inlet flow
intercooler	air inter-cooler in the compressor
out	outlet flow
ph	physical exergy
Q	thermal energy
wt	wind turbine

Acronyms

AC	alternating current
CAES	compressed air energy storage
DC	direct current
HRSG	heat recovery steam generator
GT	gas turbine
SOFC	solid oxide fuel cell
PV	photovoltaic
$PV-H_2-FC$	photovoltaic-hydrogen-fuel cell

References

1. Yang W-J, Aydin O (2001) Wind energy–hydrogen storage hybrid power generation. Int J Energy Res 25:449–463
2. Ashraf I, Chandra A, Sodha MS (2004) Techno-economic and environmental analysis for grid interactive solar photovoltaic power system of Lakshadweep islands. Int J Energy Res 28 1033–1042
3. Hosseini M, Dincer I, Rosen MA (2012) Thermodynamic analysis of a cycle integrating a solid oxide fuel cell and micro gas turbine with biomass gasification. 11th International conference on sustainable energy technologies (SET 2012) Vancouver, 2–5 Sept, 2012
4. Greenblatt JB, Succar S, Denkenberger DC, Williams RH, Socolow RH (2007) Baseload wind energy: modeling the competition between gas turbines and compressed air energy storage for supplemental generation. Energy Policy 35 1474–1492
5. Widén J, Wäckelgård E, Lund PD (2009) Options for improving the load matching capability of distributed photovoltaics: methodology and application to high-latitude data. Sol Energy 83 1953–1966
6. Castillo-Cagigal M, Caamaño-Martín E, Matallanas E, Masa-Bote D Gutiérrez A, Monasterio-Huelin F, Jiménez-Leube J (2011) PV self-consumption optimization with storage and active DSM for the residential sector. Sol Energy, 85 2338–2348
7. Radchik A, Skryabin I, Maisano J, Novikov A, Gazarian T (2013) Ensuring long term investment for large scale solar power stations: hedging instruments for green power. Sol Energy, 98(B) 167–179
8. Colpan CO, Hamdullahpur F, Dincer I, Yoo Y (2010) Effect of gasification agent on the performance of solid oxide fuel cell and biomass gasification systems. Int J Hydrogen Energy, 35 5001–5009
9. Bejan A, Tsatsaronis G, Moran M (1996) Thermal design and optimization. Wiley, New York

10. Munteanu I, Bratcu AI, Cutululis NA, Ceanga E (2008) Optimal control of wind energy systems toward a global approach. Springer, London
11. Şahin AD, Dincer I, Rosen MA (2006) Thermodynamic analysis of wind energy. Int J Energy Res 30 553–566
12. Hosseini M, Dincer I, Rosen MA (2013) Hybrid solar–fuel cell combined heat and power systems for residential applications: energy and exergy analyses. J Power Sour 221 372–380
13. Hosseini M, Dincer I, Rosen MA (2012) Steam and air fed biomass gasification: comparisons based on energy and exergy. Int J Hydrogen Energy 37 16446–16452
14. NCDIA (2011) Daily data report of Port Colborne, environment Canada. http://www.climate.weatheroffice.gc.ca/climateData/canada_e.html. Accessed 18 Apr 2013
15. UTM (2012) Weather data, University of Toronto Mississauga, University of Toronto Mississauga. http://www.utm.utoronto.ca. Accessed 12 June 2012